

FAST INVERSION OF THE EXPONENTIAL RADON TRANSFORM BY USING FAST LAPLACE TRANSFORMS

FREDRIK ANDERSSON* AND VIKTOR NIKITIN†

Abstract. The Fourier slice theorem used for the standard Radon transform generalizes to a Laplace counterpart when considering the exponential Radon transform. We show how to use this fact in combination with using algorithms for unequally spaced fast Laplace transforms to construct fast and accurate methods for computing, both the forward exponential Radon transform and the corresponding back-projection operator. Moreover, we show how to use this result for inverting data modeled by the exponential Radon transform, both in the case of complete and incomplete data measurements. For the case of incomplete data, we show how to formulate the reconstruction problem as a deconvolution problem that only uses standard FFT after some initial computations using Laplace transforms.

1. Introduction. Let $s \in \mathbb{R}$ and $\theta \in S^1$, where S^1 denotes the unit circle. The standard two dimensional *Radon transform* is defined as

$$\mathcal{R}f(s, \theta) = \int_{x \cdot \theta = s} f(x) dx = \int_{-\infty}^{\infty} f(s\theta + t\theta^\perp) dt,$$

and the parameters s and θ are used to parameterize the set of lines in \mathbb{R}^2 .

The *attenuated Radon transform* in \mathbb{R}^2 describes the mapping from functions f and μ to line integrals of the form

$$\int_{-\infty}^{\infty} f(s\theta + t\theta^\perp) e^{-\int_t^\infty \mu(s\theta + \tau\theta^\perp) d\tau} dt.$$

Integrals of this type appear for instance in medicine, where f describes the intensity distribution of isotopes or radiopharmaceuticals inside a tissue, and where the function μ describes the attenuation of the tissue. For the case where μ is constant within a known convex body, then the data obtained from the attenuated Radon transform can be modeled by the simpler *exponential Radon transform* [21],

$$(1.1) \quad \mathcal{R}_\mu f(s, \theta) = \int_{x \cdot \theta = s} f(x) dx = \int_{-\infty}^{\infty} f(s\theta + t\theta^\perp) dt.$$

In [16], a generalization of the Fourier slice theorem is derived for the exponential Radon transform along with an integral equation for the reconstruction problem of obtaining f given $\mathcal{R}_\mu f$. A similar integral equation is also derived in [6].

In [22], properties of the exponential Radon transform are derived, along with an inversion formula of filtered back-projection type. Fourier-Laplace aspects of the exponential Radon transform are also discussed. Since then, the exponential Radon transform and the associated inversion problem have been discussed by several authors. For instance, range conditions are discussed in [1], Cormack-type inversion formulas are discussed in [18], and an explicit formula for 180 degree data is given in [19].

One of the most popular methods of inverting the usual Radon transform is by means of the filtered back-projection method [17]. A drawback with this approach is that it has, in its standard implementation, a time complexity of N^3 , if we assume that reconstruction is made on an $N \times N$ lattice, and that the number of samples in s and θ are both of the order N . Although there are methods for fast ($\mathcal{O}(N^2 \log N)$) back-projection, cf. [3, 10, 12], most of the fast methods rely on usage of Fourier transforms, cf. [8, 9, 17].

In this paper, we make use of the Fourier-Laplace slice theorem to construct a fast $\mathcal{O}(N^2 \log N)$ using methods for unequally spaced fast Laplace transforms [4].

*Centre for Mathematical Sciences, Lund University, Box 118, SE-22100 Lund Sweden, (fa@maths.lth.se).

†Centre for Mathematical Sciences, Lund University, Box 118, SE-22100 Lund Sweden.

2. The Fourier-Laplace slice theorem and inversion in the continuous case. The adjoint associated with the exponential Radon transform (1.1) can be written

$$(2.1) \quad \mathcal{R}_\mu^* g(x) = \int_{S^1} e^{\mu x \cdot \theta^\perp} g(x \cdot \theta) d\theta,$$

cf. [22, 16]. It is a weighted integral of g over lines passing through the point x , and with $\mu = 0$ this operator is typically referred to as the back-projection operator.

The Fourier slice theorem, which relates the one dimensional Fourier transforms of Radon transformed data with the two-dimensional Fourier transform of data, is fairly straightforward to generalize so that it applies to the exponential Radon transform. To see this, consider the one-dimensional Fourier transform of the exponential Radon transform with respect to the first variable, s , of $\mathcal{R}_\mu f$:

$$(2.2) \quad \int_{-\infty}^{\infty} R_\mu f(s, \theta) e^{-2\pi i s \sigma} ds = \int_{-\infty}^{\infty} \int_{-\infty}^{\infty} f(s\theta + t\theta^\perp) e^{-2\pi i s \sigma + \mu t} ds dt$$

Let us use describe θ by means of an angle ϕ , i.e. $\theta = (\cos \phi, \sin \phi)$. By a change of variables,

$$\begin{aligned} x_1 &= s \cos(\phi) - t \sin(\phi), & s &= x_1 \cos(\phi) + x_2 \sin(\phi) \\ x_2 &= s \sin(\phi) + t \cos(\phi), & t &= -x_1 \sin(\phi) + x_2 \cos(\phi) \end{aligned}$$

(2.2) transforms into

$$\begin{aligned} & \int_{-\infty}^{\infty} R_\mu f(s, \theta) e^{-2\pi i s \sigma} ds \\ &= \int_{-\infty}^{\infty} \int_{-\infty}^{\infty} f(x_1, x_2) e^{-2\pi i \sigma (x_1 \cos(\phi) + x_2 \sin(\phi)) + \mu (-x_1 \sin(\phi) + x_2 \cos(\phi))} ds dt \\ &= \int_{-\infty}^{\infty} \int_{-\infty}^{\infty} f(x_1, x_2) e^{x_1 (-2\pi i \sigma \cos(\phi) - \mu \sin(\phi)) + x_2 (-2\pi i \sigma \sin(\phi) + \mu \cos(\phi))} ds dt \\ &= \widehat{f} \left(\sigma \cos(\phi) - \frac{i}{2\pi} \mu \sin(\phi), \sigma \sin(\phi) + \frac{i}{2\pi} \mu \cos(\phi) \right) = \widehat{f} \left(\sigma \theta + \frac{i\mu}{2\pi} \theta^\perp \right). \end{aligned}$$

This result is a generalization of the Fourier slice theorem. For more details, see [22, 16].

$\mathcal{R}_\mu f(s, \theta)$ can thus be obtained by a inverse one-dimensional Fourier transform of \widehat{f} ,

$$(2.3) \quad \begin{aligned} \mathcal{R}_\mu f(s, \theta) &= \int_{-\infty}^{\infty} \widehat{f} \left(\sigma \theta + \frac{i\mu}{2\pi} \theta^\perp \right) e^{2\pi i s \sigma} d\sigma \\ &= \int_{-\infty}^{\infty} \int_{\mathbb{R}^2} f(x) e^{x \cdot (-2\pi i \sigma \theta + \mu \theta^\perp) + 2\pi i s \sigma} dx d\sigma \end{aligned}$$

From this relation it immediately follows that

$$(2.4) \quad \mathcal{R}_\mu^* g(x) = \int_{-\infty}^{\infty} \int_{S^1} g(s, \theta) e^{x \cdot (2\pi i \sigma \theta + \mu \theta^\perp) - 2\pi i s \sigma} d\theta ds.$$

A reconstruction formula for the exponential Radon transform then formally reads

$$(2.5) \quad f(x) = \mathcal{R}_{-\mu}^* \mathcal{W} \mathcal{R}_\mu f,$$

where \mathcal{W} denotes the convolution operator

$$(2.6) \quad \mathcal{W}g(s, \theta) = -\frac{1}{(2\pi)^2} \int_{-\infty}^{\infty} \frac{\cos(\mu(s - \tilde{s}))}{s - \tilde{s}} \frac{\partial}{\partial \tilde{s}} g(\tilde{s}, \theta) d\tilde{s}.$$

The above integral is to be interpreted in terms of principal values. The Fourier multiplier \widehat{w} associated with \mathcal{W} is given by

$$(2.7) \quad \widehat{w}(\sigma) = \begin{cases} \frac{|\sigma|}{(2\pi)^2} & \text{if } |\sigma| \geq \frac{\mu}{2\pi} \\ 0 & \text{otherwise.} \end{cases}$$

For details about this result, we refer to [22].

It is interesting to consider the structure of the formula (2.5) a bit more in detail. In the remainder of this section we make formal arguments and ignore the functional analysis about which requirements that are needed for convergence, for being able to use Fubini's theorem etc.

Assume that we replace \mathcal{W} in (2.5) with a convolution operator in s with kernel $v(s, \theta)$ which may have depend on θ . Let \widehat{v} denote the Fourier transform of v with respect to s , and consider the operator

$$\mathcal{T}_v f = \mathcal{R}_{-\mu}^* \int_{-\infty}^{\infty} v(s - \tilde{s}, \theta) \mathcal{R}_{\mu} f(\tilde{s}, \theta) d\tilde{s}.$$

By using (2.3-2.4) to represent \mathcal{R}_{μ} and $\mathcal{R}_{-\mu}^*$ and (formally) changing the order of integration,

$$\begin{aligned} \mathcal{T}_v f(y) &= \int_{-\infty}^{\infty} \int_{S^1} \int_{-\infty}^{\infty} v(s - \tilde{s}, \theta) \\ &\quad \times \left(\int_{-\infty}^{\infty} \int_{\mathbb{R}^2} f(x) e^{x \cdot (-2\pi i \sigma \theta - \mu \theta^\perp) + 2\pi i s \sigma} dx d\sigma d\tilde{s} e^{y \cdot (2\pi i \sigma \theta + \mu \theta^\perp) - 2\pi i \tilde{s} \sigma} \right) d\tilde{s} d\theta ds. \\ &= \int_{\mathbb{R}^2} \int_{-\infty}^{\infty} \int_{S^1} \widehat{v}(\sigma, \theta) f(x) e^{(y-x) \cdot (2\pi i \sigma \theta + \mu \theta^\perp)} d\theta d\sigma dx. \\ &= T_v * f(y), \end{aligned}$$

where

$$T_v(x) = \int_{-\infty}^{\infty} \int_{S^1} \widehat{v}(\sigma, \theta) e^{x \cdot (2\pi i \sigma \theta + \mu \theta^\perp)} d\theta d\sigma.$$

For every choice of filter v the effect of applying \mathcal{T}_v can thus be described in terms of a convolution, where the kernel only depends on v . This result is of particular interest when v is chosen to model incomplete measurements, e.g., incomplete angles [19] or not dense enough sampling in the s -direction. Since convolutions are easy and fast to compute numerically by means of standard FFT, this observation can prove useful for designing iterative methods to remove artifacts due to incomplete sampling in a similar fashion, as was suggested for the case of unequally spaced Fourier data in, e.g., magnetic data interpolation [8], and in synthetic aperture radar [5].

3. Discretization. Assume that we have sampled $R_{\mu} f(s, \theta)$ at equally spaced points in s and θ . Specifically, let us assume that we have samples at a grid with N_s points in the s -direction and N_{θ} points in the θ -direction, and that we have complete coverage in the θ -domain, and that the coordinate system is normalized so that the spacing between lines (points in the s -direction) is one.

$$\begin{aligned} s_j &= j, \quad j = -\frac{N_s}{2}, \dots, \frac{N_s}{2} - 1, \\ \theta_l &= \frac{l}{2\pi}, \quad l = 0, \dots, N_{\theta} - 1. \end{aligned}$$

Associated with the nodes s_j are frequency nodes

$$\sigma_k = \frac{k}{N_s}, \quad k = -\frac{N_s}{2}, \dots, \frac{N_s}{2} - 1,$$

Using these nodes, we can compute a discretized version of (2.3) in two steps. First, we need to evaluate \widehat{f} at the nodes $(\sigma_k \theta_l + \mu \theta_l^\perp)$. If f is given by sampling on the lattice $[-\frac{N}{2}, \dots, \frac{N}{2} - 1] \times [-\frac{N}{2}, \dots, \frac{N}{2} - 1]$, then a discrete counterpart for the computation of $\widehat{f}(\sigma \theta + \mu \theta^\perp)$ reads

$$(3.1) \quad \widehat{f}(\sigma_k \theta_l + \mu \theta_l^\perp) = \sum_{n_1 = -\frac{N}{2}}^{\frac{N}{2}-1} \sum_{n_2 = -\frac{N}{2}}^{\frac{N}{2}-1} f(n_1, n_2) e^{(-\mu \sin(\theta_l) - 2\pi i \cos(\phi_l) \sigma_k) n_1 + (\mu \cos(\theta_l) - 2\pi i \sin(\phi_l) \sigma_k) n_2}.$$

By abuse of notation, we will use the same symbols for both the discrete and the continuous representations as long as there is no risk of misinterpretation. The imaginary part of the exponential above corresponds to a polar frequency grid, and the real part gives contribution from decaying/growing exponentials. In the absence of the real part (i.e. $\mu = 0$), sums of the above type can be approximately evaluated (with precision ϵ) in $\mathcal{O}(N^2 \log N + N_s N_\theta \log \epsilon)$ by using unequally spaced fast Fourier transforms (USFFT) [7, 11, 14]. To account for the case where $\mu \neq 0$, unequally spaced fast Laplace transforms [4] (USFLT) can instead be used, at the same computational cost as for the USFFT.

Once $\widehat{f}(\sigma_k \theta_l + \mu \theta_l^\perp)$ is computed, a discrete version of $\mathcal{R}_\mu(f)(s_j, \theta_l)$ can be obtained by one-dimensional discrete Fourier transforms

$$\mathcal{R}_\mu f(s_j, \theta_l) = \frac{1}{N_s} \sum_{k = \frac{N_s}{2}}^{\frac{N_s}{2}-1} \widehat{f}(\sigma_k \theta_l + \mu \theta_l^\perp) e^{2\pi i \sigma_k s_j}.$$

The back-projection operator \mathbb{R}_μ can be discretized in a similar way, using one-dimensional FFT operations in the s -direction along with a two-dimensional USFLT operation. Since the operators are adjoint, the order between the operations are reversed, and for the USFLT operation, it changes from a $\mathbb{Z}^2 \rightarrow \mathbb{C}^2$ operation to a $\mathbb{C}^2 \rightarrow \mathbb{Z}^2$ operation, cf. [4].

In order to make reconstructions from exponential Radon data following (2.5), it remains to discretize the convolution operator \mathcal{W} in (2.6). This is preferably done in the frequency domain, using the multiplier of (2.7). Due to the singularity at $\sigma = \frac{\mu}{2\pi}$, a standard FFT implementation will not provide high accuracy. By using optimal quadratures and one-dimensional USFFT operations, this problem can be avoided, however at some extra computational cost. We propose a simpler approach, and make use of a combination of oversampling, an end-point corrected trapezoidal rule [2] for equally spaced nodes σ where $\widehat{w}(\sigma) > 0$, along with adding a few nodes close to the singularity and using a higher order method for approximation on that (short) interval. In the simulations given in what follows, we have used an oversampling factor of 4, an 8-order end-point corrected trapezoidal rule [2, Table 1] with endpoint weights

$$\frac{1}{120960} [-23681, 55688, -66109, 57024, -31523, 9976, -1375],$$

and Simpson's 3/8-rule for the short interval between the discontinuity in w and the node in σ where $w(\sigma) > 0$.

We illustrate the performance of the proposed algorithm on some examples. First, we model some forward problems and compare the accuracy obtained by using the fast Laplace transform approach to using line integration with cubic interpolation.

We use a Gaussian function

$$f(x_1, x_2) = e^{-\kappa((x_1 - y_1)^2 + (x_2 - y_2)^2)},$$

centered at (y_1, y_2) , with $\kappa > 0$ for which we have the explicit formula

$$\begin{aligned} \mathcal{R}_\mu f(s, \theta) = & \\ & \exp\left(-\frac{1}{4\kappa}(8\kappa^2 \sin(\theta)v_1 \cos(\theta)v_2 + 4\kappa \sin(\theta)v_1\mu - 8\kappa^2 s \sin(\theta)v_2 - 4\kappa \cos(\theta)v_2\mu \right. \\ & \left. - 4 \cos(\theta)^2 \kappa^2 v_2^2 + 4\kappa^2 v_1^2 \cos(\theta)^2 - \mu^2 + 4\kappa^2 s^2 - 8\kappa^2 s \cos(\theta)v_1 + 4\kappa^2 v_2^2)\right) * \sqrt{\frac{\pi}{\kappa}}. \end{aligned}$$

We can also discretize the calculation of line integrals in (1.1) by cubic interpolation from the equally spaced samples in f , to points along lines to discretize

$$(3.2) \quad R_\mu f(s_j, \theta_l) \approx \delta t \sum_m f(s_j \cos(\theta_l) - t_m \sin(\theta_l), s_j \sin(\theta_l) + t_m \cos(\theta_l)) e^{\mu t_m}.$$

Figure 1 shows the approximation accuracy of $\mathcal{R}_\mu f$ for the discretized line integration and the USFLT method. We see that the error in the computation of $\mathcal{R}_\mu f$ is substantially smaller when using the USFLT compared to using the discretized line integration, and in addition with a time complexity that is favorable for the USFLT method.

We now focus on the inversion using (2.5). One practical issue that needs to be addressed is that we assume both that data is measured and reconstructed on an equally spaced, quadratic lattice. On the other hand, the sampling of the (exponential) Radon transformed data is in terms of polar lattices. While doing reconstruction, we will therefore choose either to work with oversampling in order to inscribe the quadratic lattices (in space and (complex) frequency) in larger polar grids, or to undersample so that the polar grids are instead inscribed in the quadratic lattices. The situation that is most indicative to how the method performs is, in our opinion, the case where we can assume that the support of the function we work with is inside a circle (of radius $N/2$) while the frequency content if this function is essentially also contained in a circle (of radius $1/2$). Clearly both conditions cannot be strictly satisfied at the same time due to the uncertainty principle, but they can certainly be satisfied if we loosen the conditions and satisfy with numerical compact support (i.e. that the functions are smaller in absolute value than some prescribed value outside of the circles of support mentioned above). The Gaussian example in Figure 1 is a good example of this.

To illustrate accuracy of the suggested implementation of (2.5), we conduct some examples on the *Shepp-Logan* [20] phantom. We use the modified version available in the MATLAB function *phantom*. The function f used is illustrated in the left panel of Figure 2. The phantom consists of linear combinations of characteristic functions of ellipses, and its support is inscribed in a circle. As its Fourier transform is not rapidly decaying, we apply a smooth filter to remove contribution from frequencies outside a circle of radius $1/2$. The left panel of Figure 2 shows this filtered version of the phantom.

We assume that we have access to 360° of data, and we assume that we have sufficiently dense sampling for reconstruction, specifically we use parameters $N_s = 3/2N$ and $N_\theta = 3N$. The middle panel of 2 shows the reconstruction using (2.5) and the USFLT discretization discussed in this section. The right panel shows the error between the original (filtered) data and the reconstruction, amplified by a factor 10^4 .

4. Incomplete data. We now focus on the case where the data sampling is not sufficiently dense, or not complete enough for being able to use (2.5). Typical such cases of interest concern limited angle (i.e. only 180° as discussed in [19]), the case of missing angle, or when the sampling in the s -direction is not dense enough.

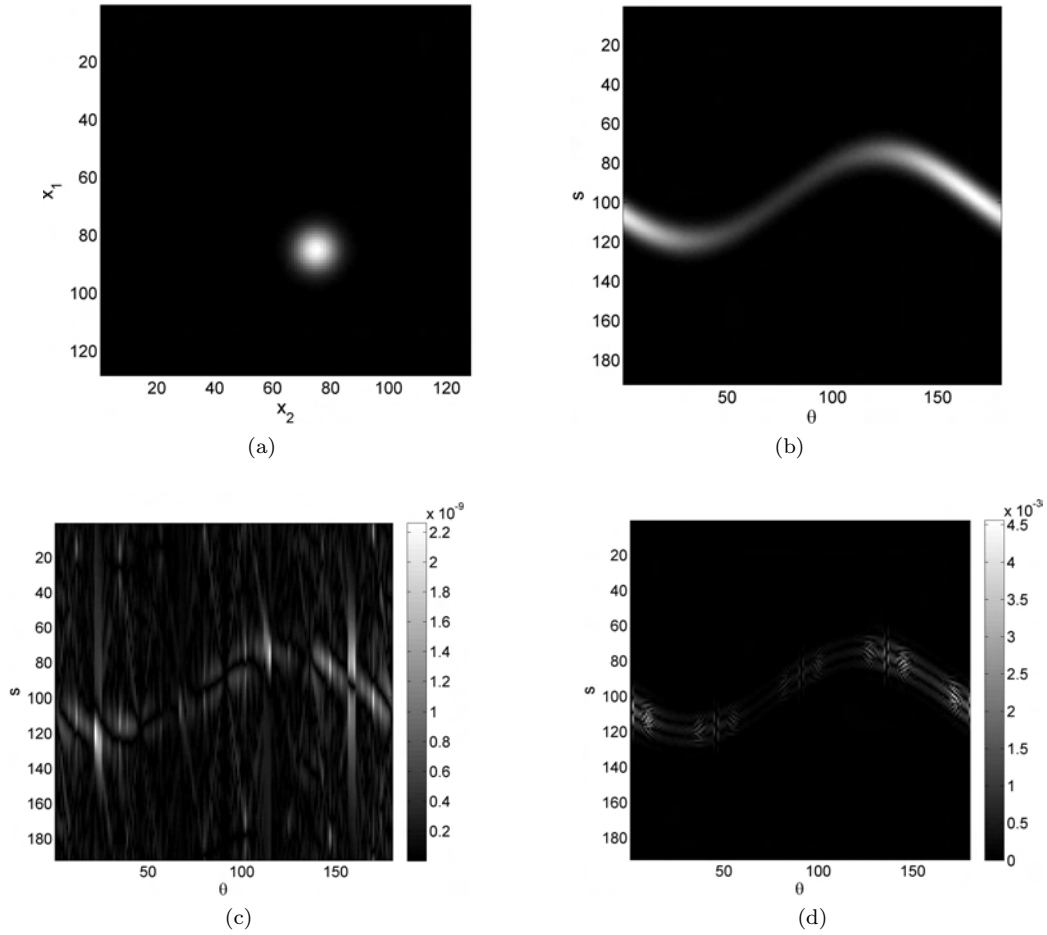


Fig. 1: (a) - Gaussian with parameters $N = 128, \kappa = 0.02, (y_1, y_2) = (10, 20)$, (b) - exponential Radon transform with parameters $N_s = 192, N_\theta = 180, \mu = \frac{2}{N}$. Comparison with analytical formula for the forward transform: (c) - approximation error when using USFLT, (d) - approximation error when using line integration.



Fig. 2: Reconstruction using 360° of exponential Radon data. The original image is shown in the left panel, and the corresponding reconstruction is shown in the middle panel, with the gray scale indicating variations between $[0, 1]$. The error between is depicted in the right panel, where the gray scale now shows errors in the range $[0, 10^{-4}]$.

As mentioned in the end of Section 2, we can model missing data by choosing a weight function v , and associated with this choice is a convolution operator \mathcal{T}_v . If the discrete filtering step consists of simple multiplication – in contrast to the modifications (end-point correction and oversampling) done for w in (2.7), and if (3.1) is used for the discretization of the Fourier-Laplace transform, then the corresponding discrete version of the operator \mathcal{K}_v will be a Toeplitz operator with kernel (point spread function)

$$T_v(n_1, n_2) = \sum_{k,l} \widehat{v}(\sigma_k, \theta_l) e^{x \cdot (2\pi i \sigma_k \theta_l + \mu \theta_l^+)} \quad n_1, n_2 = -N, \dots, N-1.$$

The reconstruction problem will then be

$$(4.1) \quad \mathcal{T}_v f = \mathcal{R}_{-\mu}^*(v *^s g), \quad \text{where } g = \mathcal{R}_\mu f.$$

For the computation of $\mathcal{R}_{-\mu}^*(v *^s g)(x)$ we use USFLT and one-dimensional FFT's. Note that the Toeplitz operator \mathcal{T}_v will in general not be positive definite.

An initial assumption of the function f was that its support was contained in a circle with radius $N/2$. This condition will typically not be satisfied for (4.1), since the point spread function T_v will typically not have compact support. However, we can incorporate the constraint in the reconstruction procedure. Let the operator χ_D denote multiplication with the characteristic function of the disc centered at the origin with radius $N/2$, and let us rephrase (4.1) into

$$(4.2) \quad \chi_D \mathcal{T}_v \chi_D f = \chi_D \mathcal{R}_{-\mu}^*(v *^s g).$$

Since the Toeplitz operator can be rapidly evaluated by means of standard FFT (see [13, p202] and [5] for a similar application), we can now try to solve (4.2) by using iterative methods. The simplest method is to use the conjugated gradient method applied to the normal equations (CGN) and solve

$$(4.3) \quad \chi_D \mathcal{T}_v \chi_D \mathcal{T}_v^* \chi_D f = \chi_D \mathcal{T}_v^* \chi_D \mathcal{R}_{-\mu}^*(v *^s g).$$

See [15] for a comparison of commonly used iterative methods for solving non-symmetric systems of linear equations.

In Figure 3 we display some results for the case where data is only available for 180° . Again, we consider results using the Shepp–Logan phantom. We also include the reconstruction obtained by ignoring the decay parameter μ in the reconstruction procedure.

The top left panel of Figure 3 depicts the result obtained when applying $\mathcal{R}_{-\mu}^*(v *^s g)$ to the measured data g , where we have used

$$\widehat{v}(\sigma, \theta) = \begin{cases} |\sigma| & \text{if } |\sigma| \geq \frac{\mu}{2\pi} \text{ and } 0 < \theta < \pi \\ 0 & \text{otherwise.} \end{cases}$$

We note that there are some low-frequency errors in the reconstruction, as well as some vertical artifacts. The grayscale color scheme used in the images of the phantom represent values in the range $[0, 1]$, and in this particular case, the low-frequent errors make some of the details fall outside of the color range. However, the reconstruction can be seen in the bottom left panel of Figure 3, depicting variations in the range $[0, 1]$.

The top right panel of Figure 3 depicts the result obtained when applying the standard Radon inversion $\mathcal{R}_0^*(v *^s g)$ to the measured data g . In this case $\widehat{v}(\sigma, \theta) = \frac{|\sigma|}{(2\pi)^2}$. The reconstruction error for this method can be seen in the bottom right panel, also depicting variations in the range $[0, 1]$.

The middle panel of Figure 3 shows the reconstruction result after 500 iterations of the conjugated gradient applied to (4.3). This reconstruction outperforms the other two in terms of quality. The reconstruction error is shown for this case in the middle lower panel, but in this case variations in the range $[0, 10^{-2}]$ are shown.

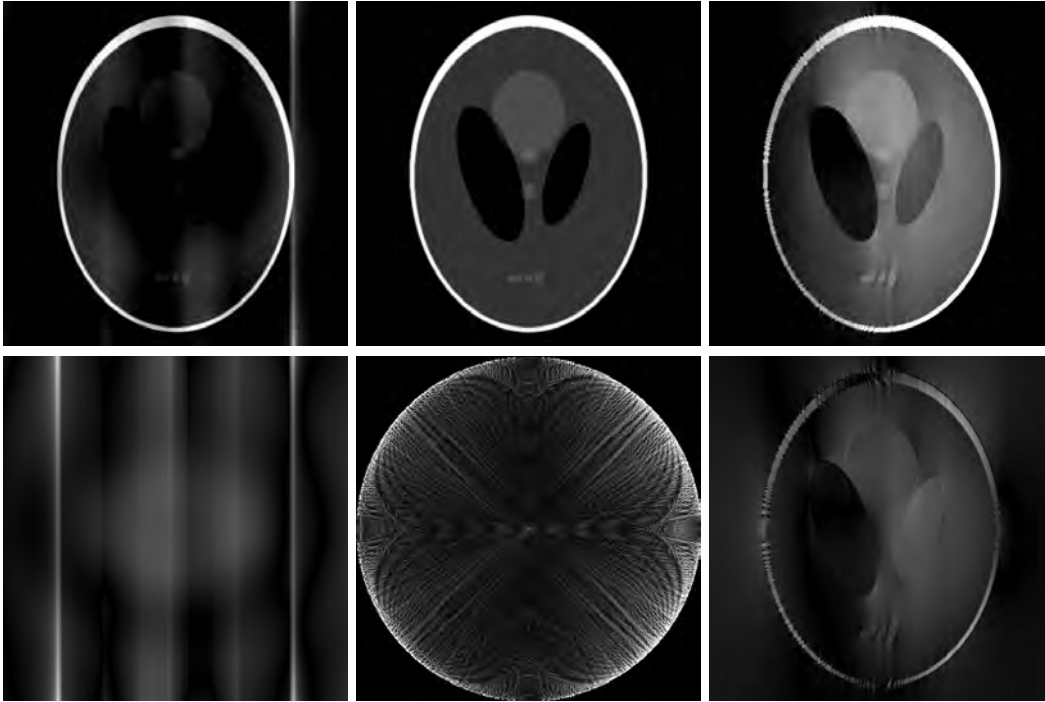


Fig. 3: Reconstruction using 180° of exponential Radon data. The original image is the same one as used in the left panel of Figure 2. The top left panel shows the result after applying the reconstruction (2.5) to the incomplete data set; the top middle panel is the result after iteratively solving the corresponding deconvolution problem 4.1; the top right panel is the result after applying the standard inversion for the Radon transform (i.e. using $\mu = 0$). The three lower panels show the corresponding absolute errors. The gray scales used in the bottom left and right panels indicate variations between $[0, 1]$, whereas the bottom middle panel indicates variation between $[0, 10^{-2}]$.

5. Conclusions. We have shown how to construct fast algorithms for the computation of the exponential Radon transform and the associated (adjoint) back-projection operator by using algorithms for fast Laplace transforms. We show how to construct numerical schemes for inversion in this case. In cases where there is not sufficient data for standard inversion formulas to apply, we show that we can reformulate the reconstruction problem in terms of a two-dimensional Toeplitz operator. Toeplitz operators can be applied rapidly by employing standard fast Fourier transforms. Hence, we can make use of iterative methods to solve the corresponding deconvolution problem, after the right hand side and the point spread function have been computed by using fast Laplace transforms.

6. Acknowledgements. This research has been supported by the Craaford Foundation, the Swedish Foundation for International Cooperation in Research and Higher Education, the Swedish Research Council and the members of the Geomathematical Imaging Group: BGP, ExxonMobil, PGS, Statoil and Total.

REFERENCES

- [1] Valentina Aguilar, Leon Ehrenpreis, and Peter Kuchment. Range conditions for the exponential Radon transform. *Journal d'Analyse Mathématique*, 68(1):1–13, 1996.
- [2] Bradley K Alpert. High-order quadratures for integral operators with singular kernels. *Journal of computational and applied mathematics*, 60(3):367–378, 1995.

- [3] Fredrik Andersson. Fast inversion of the Radon transform using log-polar coordinates and partial back-projections. *SIAM Journal on Applied Mathematics*, 65(3):818–837, 2005.
- [4] Fredrik Andersson. Algorithms for unequally spaced fast Laplace transforms. *Applied and Computational Harmonic Analysis*, 2012.
- [5] Fredrik Andersson, Randolph Moses, and Frank Natterer. Fast Fourier methods for synthetic aperture radar imaging. *Aerospace and Electronic Systems, IEEE Transactions on*, 48(1):215–229, 2012.
- [6] Gregory Beylkin. The inversion problem and applications of the generalized Radon transform. *Communications on pure and applied mathematics*, 37(5):579–599, 1984.
- [7] Gregory Beylkin. On the fast Fourier transform of functions with singularities. *Appl. Comput. Harmon. Anal.*, 2(4):363–381, 1995.
- [8] Gregory Beylkin. On applications of unequally spaced fast Fourier transform. *Mathematical Geophysics Summer School, Stanford*, 1998.
- [9] Achi Brandt, Jordan Mann, Matvei Brodski, and Meirav Galun. A fast and accurate multilevel inversion of the Radon transform. *SIAM Journal on Applied Mathematics*, 60(2):437–462, 2000.
- [10] P-E Danielsson and Malin Ingerhed. Backprojection in $\mathcal{O}(n^2 \log n)$ time X-ray CT image reconstruction. In *Nuclear Science Symposium, 1997. IEEE*, volume 2, pages 1279–1283. IEEE, 1997.
- [11] Alok Dutt and Vladimir Rokhlin. Fast Fourier transforms for nonequispaced data. *SIAM J. Sci. Comput.*, 14(6):1368–1393, 1993.
- [12] Ashvin George and Yoram Bresler. Fast tomographic reconstruction via rotation-based hierarchical backprojection. *SIAM Journal on Applied Mathematics*, 68(2):574–597, 2007.
- [13] Gene H Golub and Charles F Van Loan. *Matrix computations*, volume 3. JHUP, 2012.
- [14] Leslie Greengard and June-Yub Lee. Accelerating the nonuniform fast Fourier transform. *SIAM Review*, 46:443–454, 2004.
- [15] Noël M Nachtigal, Satish C Reddy, and Lloyd N Trefethen. How fast are nonsymmetric matrix iterations? *SIAM Journal on Matrix Analysis and Applications*, 13(3):778–795, 1992.
- [16] Frank Natterer. On the inversion of the attenuated Radon transform. *Numerische Mathematik*, 32(4):431–438, 1979.
- [17] Frank Natterer. Computerized tomography. In *The Mathematics of Computerized Tomography*, pages 1–8. Springer, 1986.
- [18] Alfred Puro. Cormack-type inversion of exponential Radon transform. *Inverse Problems*, 17(1):179, 2001.
- [19] Hans Rullgård. An explicit inversion formula for the exponential Radon transform using data from 180° . *Arkiv för matematik*, 42(2):353–362, 2004.
- [20] Lawrence A Shepp and Benjamin F Logan. The Fourier reconstruction of a head section. *IEEE Trans. Nucl. Sci.*, 21(3):21–43, 1974.
- [21] Oleh Tretiak and P Delaney. The exponential convolution algorithm for emission computed axial tomography, a review of information processing in medical imaging. Technical report, Oak Ridge National Laboratory ORNL/BCTIC2, 1978.
- [22] Oleh Tretiak and Charles Metz. The exponential Radon transform. *SIAM Journal on Applied Mathematics*, 39(2):341–354, 1980.